HHS Public Access

Author manuscript

Neuroimage. Author manuscript; available in PMC 2025 September 12.

Published in final edited form as:

Neuroimage. 2025 September ; 318: 121393. doi:10.1016/j.neuroimage.2025.121393.

Oscillatory and evoked neural responses underlying gating in the primary somatosensory cortices: Evidence from optically-pumped magnetometry

Yasra Arif[a,*], **Elizabeth Heinrichs-Graham**[a,b], **Alexa M. Wildy**[a], **Thomas W. Ward**[a,b], **Augusto Diedrich**[a,b], **Christine M. Embury**[a], **Maggie P. Rempe**[a,c], **Ryan J. Glesinger**[a], **Zhiying Shen**[a,b], **Kellen M. McDonald**[a,b], **Peihan J. Huang**[a,b], **Seth Bashford**[a], **Brittany K. Taylor**[a,b], **Max J. Kurz**[a,b], **Tony W. Wilson**[a,b]

[a]Institute for Human Neuroscience, Boys Town National Research Hospital, Boys Town, NE, 68010, USA

[b]Department of Pharmacology & Neuroscience, Creighton University, Omaha, NE, 68178, USA

[c]College of Medicine, University of Nebraska Medical Center (UNMC), Omaha, NE, 68198, USA

Abstract

Sensory gating (SG) is a protective mechanism that prevents sensory overload by attenuating neural responses to repeated stimuli while allowing allocation of neural resources to salient inputs. While studies using conventional, cryogenic magnetoencephalography (MEG) have provided a foundational understanding of the neurophysiological spectro-temporal profile of sensory gating in somatosensory cortices, its utility in diverse populations is constrained by technical limitations, including movement restriction and a one-size-fits-all helmet design. Recent developments in optically pumped magnetometry (OPM) aim to overcome these constraints by providing greater tolerance to movement and customizable helmet sizes. A small number of studies have documented the reliability of OPM in mapping somatosensory responses to median

[*]Corresponding author at: Institute for Human Neuroscience, Boys Town National Research Hospital, Omaha, NE 68010, USA. yasra.arif@boystown.org (Y. Arif).

CRediT authorship contribution statement

Yasra Arif: Writing – review & editing, Writing – original draft, Visualization, Validation, Software, Resources, Project administration, Methodology, Investigation, Formal analysis, Data curation, Conceptualization. **Elizabeth Heinrichs-Graham:** Writing – review & editing, Resources, Project administration, Methodology, Investigation, Funding acquisition, Data curation, Conceptualization. **Alexa M. Wildy:** Writing – review & editing, Project administration, Methodology, Investigation, Data curation. **Thomas W. Ward:** Writing – review & editing, Project administration, Methodology, Investigation, Formal analysis, Data curation. **Augusto Diedrich:** Writing – review & editing, Project administration, Methodology, Investigation, Data curation. **Christine M. Embury:** Writing – review & editing, Resources, Project administration, Methodology, Investigation, Data curation, Conceptualization. **Maggie P. Rempe:** Writing – review & editing, Visualization, Resources, Project administration, Methodology, Investigation, Formal analysis, Data curation. **Ryan J. Glesinger:** Writing – review & editing, Project administration, Methodology, Investigation, Data curation. **Zhiying Shen:** Writing – original draft, Methodology, Investigation, Formal analysis. **Kellen M. McDonald:** Writing – review & editing, Methodology, Investigation, Formal analysis. **Peihan J. Huang:** Writing – review & editing, Software, Resources, Methodology. **Seth Bashford:** Writing – review & editing, Validation, Software, Methodology, Data curation. **Brittany K. Taylor:** Writing – review & editing, Methodology, Investigation, Funding acquisition. **Max J. Kurz:** Writing – review & editing, Methodology, Investigation, Funding acquisition. **Tony W. Wilson:** Writing – review & editing, Visualization, Validation, Supervision, Resources, Methodology, Investigation, Funding acquisition, Conceptualization.

Declaration of competing interest

The authors of this manuscript acknowledge no conflicts of interest, financial or otherwise.

nerve stimulation using OPM; however, none have examined SG. In this study, we utilized a whole-head 128-channel OPM system and a paired-pulse median nerve stimulation paradigm to examine somato-SG and map the precise spectro-temporal cortical dynamics in a group of 31 healthy adults. Neural responses per stimulation were imaged in both the time-frequency and time domains, and voxel time series data were extracted to quantify the dynamics of somato-SG. Robust gating effects were observed in the peak and average neural responses within the primary somatosensory cortices, in both the oscillatory and time domains. These findings underscore OPM's ability to precisely resolve the spatiotemporal neural dynamics of somato-SG and stress the utility of OPM in examining somatosensory processes across developmental trajectories extending down to infants, as well as in clinical populations.

Keywords

Gamma; Theta; Virtual sensor; Beamformer; sLORETA

1. Introduction

Sensory gating (SG) is an extensively studied neural phenomenon that entails filtering redundant sensory inputs to facilitate efficient neural processing. It is typically assessed using a paired-pulse stimulation paradigm whereby two identical stimuli are presented in rapid succession, and the magnitude of the neural response to the second stimulus (S2: test) is significantly suppressed relative to the first stimulus (S1: conditioning); this is thought to reflect functional habituation- inhibition (Adler et al., 1993, 1992, 1982; Cromwell et al., 2008; Franks et al., 1983; Poon and Young, 2006). SG is thus a fundamental regulatory process that not only protects the brain against information overload but also directs the utilization of limited neural resources toward salient and novel stimuli. Understanding SG is crucial given its relevance for a range of neuropsychiatric and neurological disorders (Grunwald et al., 2003), with disruptions indicative of atypical sensory processing (e.g., hyper- or hypo-sensitivity (Lee and Syu, 2024; Patil and Kaple, 2023). It has been studied across multiple sensory modalities, including visual (Gawne et al., 2011), auditory (Grunwald et al., 2003; Jones et al., 2016), and somatosensory domains (Huttunen et al., 2008; Stevenson et al., 2012; Wiesman et al., 2017) in healthy as well as clinical populations. Examining neural correlates of SG across all the aforementioned modalities further our understanding of how neural inhibitory processes operate across functional domains and modality-specific marks of sensory dysfunction. Additionally, both evoked (i.e., phase-locked) and oscillatory characteristics of the associated responses have been widely studied using conventional cryogenic magnetoencephalography (MEG; Arif et al., 2021; Casagrande et al., 2021; Heinrichs-Graham et al., 2023; Pesonen et al., 2023; Proskovec et al., 2020; Spooner et al., 2018, 2019, 2020, 2021b, 2021a; Wiesman et al., 2017, 2021). Given its fine temporal and spatial precision, MEG serves as a valuable tool in accurately resolving neural activity underlying sensory and cognitive processes in real time and is ideal for capturing the temporal dynamics inherent in somato-SG.

Recent advances in biomagnetism, particularly the advent of optically pumped magnetometry (OPM), have made it possible to harness the strengths of MEG while

addressing some of its technical challenges. For instance, to operate effectively, the superconducting quantum interference devices (SQUIDs) in conventional MEG systems require extremely low temperatures (approx. −270 °C) maintained using liquid helium encapsulated within a large, rigid dewar, thus creating a minimal, best-case distance between the sensor array and the scalp (approx. 2–4 cm). Because the magnetic field strength associated with a given current decreases exponentially with distance, minimizing this distance is essential and leads to improvements in the signal-to-noise ratio (SNR) of the resulting brain signals. While a distance of 2–4 cm between the cortex and the MEG sensor array is possible in some adults, this distance is frequently much larger in pediatric samples due to their smaller head size and shorter neck (i.e., the bottom of the helmet often hits the shoulders before the top of the head reaches the top of the helmet). Furthermore, the fixed sensor array design of cryogenic MEG does not allow for movement, limiting its use in some clinical and pediatric populations. In contrast, OPM sensors can rest on the scalp within customized helmets (i.e., tailored to different head sizes, age ranges, etc.) that are placed on the participant's head, and this allows for movement and facilitates recording in a more naturalistic manner, thereby enhancing its translational applicability (Boto et al., 2017; Brickwedde et al., 2024; Brookes et al., 2022). However, OPM is a nascent technology, and replication of MEG findings using OPM is crucial for establishing its reliability.

To date, only a few studies have utilized OPM with median nerve stimulation paradigms to capture neural responses and map their origins to the somatosensory cortices using various source imaging/localization approaches. For example, Boto et al. simulated a multi-channel array by using 13 sequential placements of a single-channel OPM over the somatosensory cortex to investigate responses underlying median nerve stimulation and demonstrated localization of the evoked response (N20) reliably to the somatosensory region using a dipole model (Boto et al., 2017). A subsequent study replicated these findings using a 20-channel OPM in three participants (Borna et al., 2020). Finally, one recent study using a 28-channel OPM system in seven healthy adults and another study using a 32-channel unit in four participants reported both time-domain and time-frequency domain somatosensory responses and mapped their cortical origins, with the latter highlighting differences in the phase synchronization between rhythmic and arrhythmic stimulation of the median nerve (An et al., 2022; Ma et al., 2024). While these studies have provided critical insights, they were limited by small sample sizes and a lack of whole-head coverage. Moreover, none of these studies investigated somatosensory gating, which is an important next step considering its critical role in assessing the functional integrity of the somatosensory system, as disruptions in gating have been linked to sensory deficits relevant to multiple neurological and psychiatric conditions (Arif et al., 2021; Casagrande et al., 2022; Kurz et al., 2018; Pesonen et al., 2023; Spooner et al., 2020, 2018; Thoma et al., 2007; Trevarrow et al., 2022; Wiesman et al., 2021). In the current study, we utilized an OPM system with 128 channels and a paired-pulse median nerve stimulation paradigm to quantify somato-SG responses and spatially map their precise spectro-temporal dynamics in 31 healthy adults. Our primary hypothesis was that our paired-pulse paradigm would elicit evoked and induced oscillatory somatosensory responses that would be reliably detected and characterized using OPM, and that we would see significant somato-SG dynamics (e.g., significant suppression of

response power to S2 relative to S1), in line with findings observed in studies using the same paradigm in the context of cryogenic MEG.

2. Methods

2.1. Participants

Thirty-one right-handed healthy adults (15 females) aged 20–35 years (M = 26.72 years, SD = 4.35) were enrolled from the local community. Exclusionary criteria included any medical illness affecting the CNS, any neurologic or psychiatric disorder, history of head trauma, current substance misuse, and standard OPM exclusion criteria (e.g., dental braces, battery-operated implants, and/or any type of ferromagnetic implanted material). The Institutional Review Board (IRB) at Boys Town National Research Hospital approved the study and written informed consent was obtained from each participant after a full description of the study; all protocols were in accordance with the Declaration of Helsinki.

2.2. Experimental paradigm

Prior to OPM recording, participants were seated with their eyes closed in a non-magnetic chair with the whole-head OPM sensor array positioned on their head. Electrical stimulation was applied to the left median nerve using external cutaneous stimulators connected to a Digitimer DS7A constant-current stimulator system (Digitimer Ltd, Garden City, UK). For each participant, we collected at least 80 paired-pulse trials with an inter-stimulus interval of 500 ms and an inter-pair interval that randomly varied between 4500 and 4800 ms (Fig. 1A). Each pulse generated a 0.2 ms constant-current square wave that was set to a limit of approximately 10 % above the threshold required to elicit a subtle twitch of the thumb. Total OPM recording time was approximately 7 min per participant.

2.3. OPM data acquisition

The OPM data were collected using a 128-channel (i.e., 64 dual-axis units) magnetometer system equipped with third-generation Qu-Spin sensors (QuSpin, Inc., Louisville, Colorado, USA; Cerca Magnetics Limited, Nottingham, UK). Neuromagnetic data were sampled continuously at 1.2 kHz using a 0.1–400 Hz acquisition passband. All recordings were completed in a magnetically shielded room (MSR; MuRoom®, Magnetic Shields Limited, Staplehurst, England, UK) equipped with an array of field-nulling coils. The whole-head OPM array was configured using custom 3D-printed helmets. For this study of young adults, we used two adult-size helmets with equivalent inter-sensor spacing (i.e., spatial frequency sampling); 13 participants wore the larger helmet and 18 wore the smaller helmet, with helmet selection being based on head circumference. Prior to recording, participants were seated in the OPM chair and the door to the MSR was closed. The MSR was then degaussed and the nulling coils were energized to ensure minimal gradients in a 1 m^3 cube surrounding the OPM helmet (Holmes et al., 2023). The residual field within the nulling cube was measured continuously using two triaxial OPM sensors positioned equally spaced to the left and right of the participant at the height of the cortical array. Participants were monitored throughout OPM data acquisition via real-time audio-visual feeds from inside the shielded room. After the recording, OPM data from each participant was subjected to global noise reduction using homogenous field correction (HFC; Tierney et al., 2021). Any channels that

were defined as “bad” (i.e., noisy or dead channels) were removed from the dataset before applying HFC.

2.4. MRI data acquisition

Individual structural MRI data were obtained with a 3T Siemens Prisma MRI scanner using a 32-channel head coil and the following parameters: TR: 2400 ms; TE: 2.05 ms; field of view: 256 mm; matrix: 256 × 256; slice thickness: 1 mm; voxel size: 1.0 × 1.0 × 1.0 mm; acquisition plane: sagittal; flip angle: 8 degrees. Structural MRI data were aligned parallel to the anterior and posterior commissures, segmented, and transformed into standardized space. After source analysis, each participant’s functional images were transformed into the same standardized space using the transform applied to the structural MRI volume.

2.5. OPM coregistration & structural MRI processing

Once the helmet was positioned for OPM recording, the participant’s head, including their face, fiducial marks, and the helmet were digitally captured using a 3D optical imaging system (EinScan H, SHINING 3D, Hangzhou, China). This spatial information was used during post-processing for coregistration with structural MRI. Briefly, the 3D digital scan of the participant’s head wearing the helmet was coregistered to both the person’s MRI data using three fiducial points (i.e., nasion, left and right zygomatic bone) and a 3D rendering of the helmet geometry. In both coregistration steps (i.e., coregistration with MRI and coregistration with helmet geometry), the key registration points were highlighted by markers in the optical scan to help ensure the correct spatial points were precisely located and utilized. Since the geometry of the helmet, including the location and angle of each inherent sensor holder, was precisely known based on the CAD file used for 3D printing, the location and orientation of each magnetic sensor could be derived. Once the OPM helmet and MRI data were coregistered, a transformation matrix was computed to transform the precise sensor locations/orientations into the participant’s head space coordinates. With this coordinate system (including skin surface points derived from the aforementioned 3D optical scan), each participant’s OPM data were coregistered with their structural MRI prior to source space analyses using BESA MRI (V3.0, BESA GmbH, Gräfelfing, Germany).

2.6. OPM data pre-processing and sensor-level statistics

Cardiac artifacts were removed from the data using signal-space projection (SSP), which was accounted for during source reconstruction (Uusitalo and Ilmoniemi, 1997). Channels exhibiting excessively high amplitude and/or gradient values, inconsistent with neural data, were identified and excluded A low-cutoff filter (0.5 Hz, zero-phase, 12 dB/oct slope), a high-cutoff filter (110 Hz, zero-phase, 24 dB/oct slope), and a notch filter (60 Hz, 2 Hz width) were applied to the data. The continuous magnetic time series was divided into epochs of 3700 ms duration, with 0 ms defined as the onset of the first stimulation and the baseline being the −700 to −300 ms time window. Epochs containing artifacts were rejected based on a fixed threshold method, supplemented with visual inspection. On average, 73 trials per participant were used for further analysis. An individually determined threshold based on the signal distribution for both signal amplitude and gradient was used to reject artifacts. Across all participants, the average amplitude threshold was 33,306.45 (SD = 10,866.37) fT/cm and the average gradient threshold was 5883.87 (SD = 4757.25)

fT/(cm*ms). Across participants, an average of 73 (SD = 2.91) trials were used for further analysis.

For the time-frequency analysis, we transformed the post-artifact-rejection epochs into the time-frequency domain using complex demodulation (Kovach and Gander, 2016; Papp and Ktonas, 1977), and the resulting spectral power estimations per sensor were averaged over trials to generate time-frequency plots of mean spectral density (5 Hz, 10 ms; range: 10–100 Hz). Given the findings of significant gating at lower frequencies (Wiesman and Wilson, 2020), we also conducted an analysis targeting these oscillations (1 Hz, 50 ms; range: 4–20 Hz). In each case, these sensor-level data were normalized per time-frequency bin using the respective bin's baseline power, which was calculated as the mean power during the −700 to −300 ms time period. The time-frequency windows used for source analysis were determined by statistical analysis of the sensor-level spectrograms across the entire array of magnetometers. Each data point in the spectrograms was initially evaluated using a mass univariate approach based on the general linear model. To reduce the risk of false positive results while maintaining reasonable sensitivity, a two-stage procedure was followed to control for Type 1 error. In the first stage, paired-sample *t*-tests were conducted to test for differences between the mean baseline per frequency bin and each data point in the spectrogram following stimulus onset, and the output spectrogram of t-values was thresholded at $p < .05$ to define time-frequency bins containing potentially significant oscillatory responses across all participants. In stage two, the time-frequency bins that survived the threshold were clustered with temporally and/or spatially neighboring bins that were also above the threshold, and a cluster value was derived by summing all of the t-values of all data points in the cluster. Nonparametric permutation testing was then used to derive a distribution of cluster values, and the significance level of the observed clusters (from stage one) were tested directly using this distribution (Ernst, 2004; Maris and Oostenveld, 2007). For each comparison, 1000 permutations were computed to build a distribution of cluster values. Based on these analyses, the time-frequency windows that contained significant oscillatory events across all participants were subjected to a beamforming analysis.

To investigate the evoked responses commonly associated with somatosensory processing, the same artifact-free epochs were averaged across trials to generate a mean time series per sensor, and the specific time windows used for subsequent source analysis were again determined by means of a paired-sample cluster-based permutation test against baseline across all participants. For each comparison, 1000 permutations were computed to build a distribution of cluster values, and the time windows of time-domain evoked data that were non-exchangeable with baseline ($p < .05$) across all participants, according to these permutation analyses, were used to guide subsequent source-level analysis of the time domain signals.

2.7. OPM source analysis and statistics

Time-frequency resolved beamformer source images were computed using the dynamic imaging of coherent sources (DICS; regularization: singular value decomposition 0.0001 %; Gross et al., 2001) approach, which applies spatial filters in the time-frequency domain to

calculate voxel-wise power for the entire brain volume. The single images were derived from the cross-spectral densities of all combinations of magnetometers averaged over the time-frequency range of interest and the solution of the forward problem for each location on a grid specified by input voxel space. Following convention, we computed noise-normalized source power for each voxel per participant using active (i.e., task) and passive (i.e., baseline) periods of equal duration and bandwidth (Hillebrand et al., 2005) at a resolution of 4.0 × 4.0 × 4.0 mm. Such images are typically referred to as pseudo-t maps, with units (pseudo-t) that reflect noise-normalized power differences (i.e., active versus passive) per voxel. OPM pre-processing and imaging used the BESA research (version 7.1) software.

Images for the significant time-frequency window around each stimulation were computed separately per participant and then grand-averaged across both stimulations and all participants. Voxel time-series data (i.e., “virtual sensors”) were then extracted from each participant’s data using the peak voxel in these grand-averaged beamformer images. To compute the virtual sensors, we applied the sensor weighting matrix derived through the forward computation to the preprocessed signal vector, which yielded a time series for the specific coordinate in source space.

Note that virtual sensor extraction was done per participant once the coordinates of interest were known. Once the virtual sensor time series were extracted, we computed the envelope of the spectral power in the frequency bin that was used in the beamforming analysis. From this time series, we computed the relative (i.e., baseline-corrected) time series of each participant.

Time domain source images were computed using standardized low-resolution brain electromagnetic tomography (sLORETA; regularization: Tikhonov 0.01 %; Pascual-Marqui, 2002). The resulting whole-brain maps were 4-dimensional estimates of current density per voxel, per time sample across the experimental epoch. These data were normalized to the sum of the noise covariance and theoretical signal covariance, and thus the units are arbitrary. Using the temporal clusters identified in the sensor-level analysis, these maps were averaged over time following each somatosensory stimulation and then grand-averaged across the two stimulations to determine the peak voxel of the time-domain neural response to the stimuli across all participants. From this peak, the sLORETA units were extracted per stimulation to derive estimates of the time-domain response amplitude for each participant.

3. Results

3.1. Oscillatory and virtual sensor analyses

We initially focused on the time-frequency transformed OPM data and found significant increases relative to baseline in many sensors near the sensorimotor and parietal regions from about 10 Hz to 90 Hz during the first 100 ms after the onset of each stimulation ($p < .001$ corrected; Fig. 1B). To evaluate the dynamics and remain consistent with the traditional gamma band, we focused our beamformer analyses on the 30–75 Hz frequency range and utilized two 50 ms time intervals in which the neural response to stimulation was the strongest (0–50 ms and 500–550 ms). These time-frequency windows were imaged using

a beamforming approach, which revealed virtually identical locations in the contralateral somatosensory hand region for both the first and second stimulations (i.e., neighboring voxels that shared an edge; Fig. 1C). Next, we grand-averaged the beamformer images across both stimulations and all participants and then extracted the voxel time-series data for each participant from the peak voxel coordinates in this grand-averaged map and conducted time-frequency analyses on these voxel time series. Specifically, we computed the power envelope for the band of interest (30–75 Hz) in relative (i.e., baseline-corrected) units. The relative peak power and the average power across the beamformer time windows used for the first (0–50 ms) and second stimulations (500–550 ms) were then probed using two-tailed, paired-sample *t*-tests. These tests indicated a significant decrease of 12.05 % in the peak power response ($t = 3.131$, $p = .004$) and a decrease of 9.12 % in the averaged response ($t = 2.535$, $p = .017$) to S2 relative to S1 (Fig. 2).

Although far less common in the MEG somatosensory gating literature, given the findings of (Wiesman and Wilson, 2020), we also probed whether gating was observed in lower frequency responses. Our data indicated sensor-level responses in the theta and alpha ranges ($p < .001$ corrected). Consistent with the analysis focusing on gamma responses, we imaged the two theta responses (4–8 Hz; 0–250 ms and 500–750 ms) and the two alpha responses (9–13 Hz; 150–450 ms and 650–950 ms) and then grand-averaged each to derive the peak voxel. We observed significant gating in the theta range, but not for the alpha oscillations ($p > .50$). For theta, two-tailed paired-samples *t*-tests indicated a significant decrease of 37.42 % in the peak power response ($t = 7.657$, $p < .001$ and a decrease of 41.42 % in the averaged power response ($t = 7.978$, $p < .001$) from the first (0–250 ms) to the second stimulations (500–750 ms; Fig. 3).

3.2. Time-domain (evoked) analyses

Next, we examined the time-domain averaged data by first conducting paired *t*-tests against baseline across all participants and magnetometers to identify time periods of interest. These analyses indicated sensor-level responses from 20–180 and 525–685 ms ($p < .001$ corrected), corresponding to responses to the first and second stimulation, respectively. Next, we applied sLORETA to compute whole-brain images of the evoked responses in each participant and then averaged these images within the time periods identified in the sensor-level analysis. These images were then grand-averaged across both stimulation periods and all participants to identify the peak voxel. Note that the peak voxels across the two stimulation periods were identical. The time series of this peak voxel was then extracted. Similar to the oscillatory responses, two-tailed paired-sample *t*-tests were conducted on the peak and average response amplitudes of the first (20–180 ms) and second stimulations (525–685 ms). These tests indicated a significant mean decrease of 12.28 % in the peak response ($t = 4.147$, $p < .004$) and a reduction of 16.78 % in the averaged response ($t = 6.976$, $p < .001$) to the S2 relative to the S1 (Fig. 4).

4. Discussion

In the present study, we utilized a whole-head OPM array to demonstrate SG in the somatosensory cortices of healthy adults using paired-pulse median nerve stimulation. We

specifically observed a reduction (i.e., gating effect) in both the peak and average responses within the window of the second stimulation compared to the first, for both evoked and gamma oscillatory responses. In addition, we probed lower frequency responses and found significant gating in the theta range, but not for alpha oscillations, which is largely consistent with the limited work examining such gating in lower frequency responses (Wiesman and Wilson, 2020). These data are among the first to illustrate the potential of OPM to resolve somatosensory SG responses, offering a promising tool to investigate sensory processing deficits that have been shown in multiple clinical groups (Arif et al., 2021; Casagrande et al., 2022; 2021; Spooner et al., 2020, 2018; Trevarrow et al., 2021; Wiesman et al., 2021). Below, we discuss the implications of these findings for future work in clinical-translational settings.

Somatosensory processing deficits often co-exist with movement disorders due to direct synaptic connections and the convergence of anatomical and functional pathways (Imai et al., 2016). SG impairments and/or somatosensory processing deficits have also been reported in a myriad of disorders or diseases that also present with motor dysfunction, including but not limited to cerebral palsy (Kurz et al., 2018; Trevarrow et al., 2022; 2021), attention-deficit/hyperactivity disorder (ADHD; Frost-Karlsson et al., 2024; Micoulaud-Franchi et al., 2019; Schulze et al., 2020), autism spectrum disorder (Crasta et al., 2021; Schulz et al., 2023), Tourette syndrome (Houghton et al., 2014), schizophrenia (Thoma et al., 2007), traumatic brain injury/stroke (Staines et al., 2002), multiple sclerosis (Arpin et al., 2017), Parkinson's and Huntington's disease (Boecker et al., 1999). Investigating the underlying neural origins of deficits reliably has historically been very challenging, as participants with neurodevelopmental disabilities frequently have difficulties remaining still, while those with age-related neurological disorders generally exhibit more symptoms (e.g., excessive motor restlessness, involuntary movements) with increased severity. The inherent constraints of conventional cryogenic MEG have often limited discovery in many of these affected populations, as participant motion has a major impact on data quality. Further, the one-size-fits-all fixed helmet design has also hampered pediatric research using cryogenic MEG, as the distance between the brain and the MEG sensors in very young children and infants is often so far that the SNR of the measurements is limited, making source reconstruction of the resulting data unreliable.

Although electroencephalography (EEG) has been a long-time mainstay for recording neurophysiological data in patients and children, its limited spatial precision often puts it at a disadvantage compared to MEG. In many ways, OPM technology harnesses the best of both methods, as it circumvents the fixed array and motion problems of MEG by using an adaptable helmet design that is worn and thus allows greater tolerance to movement while also allowing the sensors to be directly placed on the scalp. Further, it overcomes the limitations of EEG in terms of spatial precision and sensitivity to higher frequency neural responses by measuring the magnetic component of the electrical fields, which is far less impacted by the skull and other intervening tissues. Thus, OPM has immense potential and may ultimately enhance our understanding of many different neuropathologies and help track disease progression by observing how somatosensory deficits evolve over time, which, in turn, could pave the way for more targeted therapeutic interventions. Additionally, OPM may offer unique insight into neurotypical and neurodiverse developmental trajectories by

enabling a much broader population to be accurately studied with advanced neuroimaging methods. The novel flexibility of OPM will also help advance ecologically valid neuroscience research by enabling neural responses to be captured in real-life settings such as social interactions, parent-child dynamics, and engagement in virtual or augmented reality simulations (Roberts et al., 2019).

To summarize, we used a novel OPM array to quantify oscillatory and evoked SG neural responses in healthy young adults. Our results demonstrate somato-SG for the first time using OPM and replicate several key SG observations from the MEG literature. Thus, our data not only support previous OPM reports that mapped somatosensory neural responses, but also extend this work by demonstrating significant SG. Despite the novelty of this study, there were limitations and future OPM work would benefit by determining whether the neural signatures of SG are modulated by attentional states, which has been shown in previous MEG work (Wiesman and Wilson, 2020). In addition to basic sensory processing, it is important to validate higher-order cognitive responses using OPM, as the complex interplay between sensory and cognitive processes can have vital implications for both health and disease. Thus, future studies should also harness higher-order cognitive tasks, as it is possible that the larger neural signals measured from the scalp by OPM could identify previously missed neural responses during working memory, attention, and executive function tasks. Another notable consideration is the use of individual-specific MRIs for source reconstruction. While using individual MRIs improves spatial precision, it may seem like a limitation to the applicability of OPM studies to traditionally ‘difficult-to-scan’ populations. However, prior research has shown that the use of a template MRI yields results that are highly comparable to those obtained using individual-specific MRIs in SQUID-MEG studies (Holliday et al., 2003; Wiesman et al., 2020; 2019; Wiesman and Wilson, 2020, 2019). As OPM technology continues to evolve, refinements such as individualized helmets designed to fit each participant’s unique head size and geometry may further advance the system’s accuracy in quantifying neural signals. Finally, extending this work to clinical and pediatric populations, as well as exploring applications beyond the sensory domain, is crucial to fully leverage the translational promise of OPM.

Acknowledgments

This work was supported by the National Institutes of Health [grant numbers: P20-GM144641 (EHG, BKT, MJK, and TWW), S10-OD032468 (EHG, BKT, MJK, and TWW), R01-DA059542 (TWW).

Data availability

The data used in this article will be made publicly available through the COINS framework at the completion of the study (https://coins.trendscenter.org/).

References

Adler LE, Hoffer LD, Wiser A, Freedman R, 1993. Normalization of auditory physiology by cigarette smoking in schizophrenic patients. Am. J. Psychiatry 150, 1856–1861. 10.1176/ajp.150.12.1856. [PubMed: 8238642]

Adler LE, Hoffer LJ, Griffith J, Waldo MC, Freedman R, 1992. Normalization by nicotine of deficient auditory sensory gating in the relatives of schizophrenics. Biol. Psychiatry 32, 607–616. 10.1016/0006-3223(92)90073-9. [PubMed: 1450287]

Adler LE, Pachtman E, Franks RD, Pecevich M, Waldo MC, Freedman R, 1982. Neurophysiological evidence for a defect in neuronal mechanisms involved in sensory gating in schizophrenia. Biol. Psychiatry 17, 639–654. [PubMed: 7104417]

An N, Cao F, Li W, Wang W, Xu W, Wang C, Xiang M, Gao Y, Sui B, Liang A, Ning X, 2022. Imaging somatosensory cortex responses measured by OPM-MEG: variational free energy-based spatial smoothing estimation approach. iScience 25, 103752. 10.1016/j.isci.2022.103752. [PubMed: 35118364]

Arif Y, Wiesman AI, Christopher-Hayes NJ, Wilson TW, 2021. Aberrant inhibitory processing in the somatosensory cortices of cannabis-users. J. Psychopharmacol 35, 1356–1364. 10.1177/02698811211050557. [PubMed: 34694190]

Arpin DJ, Gehringer JE, Wilson TW, Kurz MJ, 2017. A reduced somatosensory gating response in individuals with multiple sclerosis is related to walking impairment. J. Neurophysiol 118, 2052–2058. 10.1152/jn.00260.2017. [PubMed: 28724780]

Boecker H, Ceballos-Baumann A, Bartenstein P, Weindl A, Siebner HR, Fassbender T, Munz F, Schwaiger M, Conrad B, 1999. Sensory processing in Parkinson's and Huntington's disease: investigations with 3D H215O-PET. Brain 122, 1651–1665. 10.1093/brain/122.9.1651. [PubMed: 10468505]

Borna A, Carter TR, Colombo AP, Jau Y-Y, McKay J, Weisend M, Taulu S, Stephen JM, Schwindt PDD, 2020. Non-invasive functional-brain-imaging with an OPM-based magnetoencephalography system. PLoS One 15, e0227684. 10.1371/journal.pone.0227684. [PubMed: 31978102]

Boto E, Meyer SS, Shah V, Alem O, Knappe S, Kruger P, Fromhold TM, Lim M, Glover PM, Morris PG, Bowtell R, Barnes GR, Brookes MJ, 2017. A new generation of magnetoencephalography: room temperature measurements using optically-pumped magnetometers. Neuroimage 149, 404–414. 10.1016/j.neuroimage.2017.01.034. [PubMed: 28131890]

Brickwedde M, Anders P, Kühn AA, Lofredi R, Holtkamp M, Kaindl AM, Grent-'t-Jong T, Krüger P, Sander T, Uhlhaas PJ, 2024. Applications of OPM-MEG for translational neuroscience: a perspective. Transl. Psychiatry 14, 1–12. 10.1038/s41398-024-03047-y. [PubMed: 38172115]

Brookes MJ, Leggett J, Rea M, Hill RM, Holmes N, Boto E, Bowtell R, 2022. Magnetoencephalography with optically pumped magnetometers (OPM-MEG): the next generation of functional neuroimaging. Trends Neurosci. 45, 621–634. 10.1016/j.tins.2022.05.008. [PubMed: 35779970]

Casagrande CC, Lew BJ, Taylor BK, Schantell M, O'Neill J, May PE, Swindells S, Wilson TW, 2021. Impact of HIV-infection on human somatosensory processing, spontaneous cortical activity, and cortical thickness: a multimodal neuroimaging approach. Hum. Brain Mapp 42, 2851–2861. 10.1002/hbm.25408. [PubMed: 33738895]

Casagrande CC, Wiesman AI, Schantell M, Johnson HJ, Wolfson SL, O'Neill J, Johnson CM, May PE, Swindells S, Murman DL, Wilson TW, 2022. Signatures of somatosensory cortical dysfunction in Alzheimer's disease and HIV-associated neurocognitive disorder. Brain Commun. 4, fcac169. 10.1093/braincomms/fcac169. [PubMed: 35813878]

Crasta JE, Gavin WJ, Davies PL, 2021. Expanding our understanding of sensory gating in children with autism spectrum disorders. Clin. Neurophysiol 132, 180–190. 10.1016/j.clinph.2020.09.020. [PubMed: 33310588]

Cromwell HC, Mears RP, Wan L, Boutros NN, 2008. Sensory gating: a translational effort from basic to clinical science. Clin. EEG Neurosci 39, 69–72. 10.1177/155005940803900209. [PubMed: 18450171]

Ernst MD, 2004. Permutation methods: a basis for exact inference. Statist. Sci 676–685.

Franks RD, Adler LE, Waldo MC, Alpert J, Freedman R, 1983. Neurophysiological studies of sensory gating in mania: comparison with schizophrenia. Biol. Psychiatry 18, 989–1005. [PubMed: 6416309]

Frost-Karlsson M, Capusan AJ, Olausson H, Boehme R, 2024. Altered somatosensory processing in adult attention deficit hyperactivity disorder. BMC Psychiatry 24, 558. 10.1186/s12888-024-06002-9. [PubMed: 39138461]

Gawne TJ, Osbourne TS, Risner ML, 2011. Robust sensory gating in the cortical visual evoked potential using two spatially separated stimuli. Clin. Neurophysiol 122, 588–593. 10.1016/j.clinph.2010.07.015. [PubMed: 20709595]

Gross J, Kujala J, Hämäläinen M, Timmermann L, Schnitzler A, Salmelin R, 2001. Dynamic imaging of coherent sources: studying neural interactions in the human brain. Proc. Natl. Acad. Sci 98, 694–699. [PubMed: 11209067]

Grunwald T, Boutros NN, Pezer N, von Oertzen J, Fernández G, Schaller C, Elger CE, 2003. Neuronal substrates of sensory gating within the human brain. Biol. Psychiatry 53, 511–519. 10.1016/s0006-3223(02)01673-6. [PubMed: 12644356]

Heinrichs-Graham E, Walker EA, Lee WH, Benavente AA, McCreery RW, 2023. Somatosensory gating is related to behavioral and verbal outcomes in children with mild-to-severe hearing loss. Cereb. Cortex 33, 5228–5237. 10.1093/cercor/bhac412. [PubMed: 36310092]

Hillebrand A, Singh KD, Holliday IE, Furlong PL, Barnes GR, 2005. A new approach to neuroimaging with magnetoencephalography. Hum. Brain Mapp 25, 199–211. [PubMed: 15846771]

Holliday IE, Barnes GR, Hillebrand A, Singh KD, 2003. Accuracy and applications of group MEG studies using cortical source locations estimated from participants' scalp surfaces. Hum. Brain Mapp 20, 142–147. 10.1002/hbm.10133. [PubMed: 14601140]

Holmes N, Rea M, Hill RM, Leggett J, Edwards LJ, Hobson PJ, Boto E, Tierney TM, Rier L, Rivero GR, Shah V, Osborne J, Fromhold TM, Glover P, Brookes MJ, Bowtell R, 2023. Enabling ambulatory movement in wearable magnetoencephalography with matrix coil active magnetic shielding. Neuroimage 274, 1–14. 10.1016/j.neuroimage.2023.120157.

Houghton DC, Capriotti MR, Conelea CA, Woods DW, 2014. Sensory phenomena in Tourette syndrome: their role in symptom formation and treatment. Curr. Dev. Disord. Rep 1, 245–251. 10.1007/s40474-014-0026-2. [PubMed: 25844305]

Huttunen J, Pekkonen E, Kivisaari R, Autti T, Kähkönen S, 2008. Modulation of somatosensory evoked fields from SI and SII by acute GABAA-agonism and paired-pulse stimulation. Neuroimage 40, 427–434. 10.1016/j.neuroimage.2007.12.024. [PubMed: 18234513]

Imai F, Ladle DR, Leslie JR, Duan X, Rizvi TA, Ciraolo GM, Zheng Y, Yoshida Y, 2016. Synapse formation in monosynaptic sensory–Motor connections is regulated by presynaptic Rho GTPase Cdc42. J. Neurosci 36, 5724–5735. 10.1523/JNEUROSCI.2146-15.2016. [PubMed: 27225763]

Jones LA, Hills PJ, Dick KM, Jones SP, Bright P, 2016. Cognitive mechanisms associated with auditory sensory gating. Brain Cogn. 102, 33–45. 10.1016/j.bandc.2015.12.005. [PubMed: 26716891]

Kovach CK, Gander PE, 2016. The demodulated band transform. J. Neurosci. Methods 261, 135–154. 10.1016/j.jneumeth.2015.12.004. [PubMed: 26711370]

Kurz MJ, Wiesman AI, Coolidge NM, Wilson TW, 2018. Children with cerebral palsy hyper-gate somatosensory stimulations of the foot. Cereb. Cortex 28, 2431–2438. 10.1093/cercor/bhx144. [PubMed: 28591842]

Lee BD, Syu Y-C, 2024. Atypical sensory processing, sensory gating, and participation for adults with Schizophrenia spectrum disorders: a scoping review. Occup. Ther. Ment. Health 40, 177–192. 10.1080/0164212X.2023.2251685.

Ma Y-Y, Gao Y, Wu H-Q, Liang X-Y, Li Y, Lu H, Liu C-Z, Ning X-L, 2024. OPM-MEG measuring phase synchronization on source time series: application in rhythmic median nerve stimulation. IEEE Trans. Neural. Syst. Rehabil. Eng 32, 1426–1434. 10.1109/TNSRE.2024.3381173. [PubMed: 38530717]

Maris E, Oostenveld R, 2007. Nonparametric statistical testing of EEG-and MEG-data. J. Neurosci. Methods 164, 177–190. [PubMed: 17517438]

Micoulaud-Franchi J-A, Lopez R, Cermolacce M, Vaillant F, Péri P, Boyer L, Richieri R, Bioulac S, Sagaspe P, Philip P, Vion-Dury J, Lancon C, 2019. Sensory gating capacity and attentional function in adults with ADHD: a preliminary neurophysiological and neuropsychological study. J. Atten. Disord 23, 1199–1209. 10.1177/1087054716629716. [PubMed: 26896149]

Papp N, Ktonas P, 1977. Critical evaluation of complex demodulation techniques for the quantification of bioelectrical activity. Biomed. Sci. Instrum 13, 135–145. [PubMed: 871500]

Pascual-Marqui RD, 2002. Standardized low-resolution brain electromagnetic tomography (sLORETA): technical details. Methods Find. Exp. Clin. Pharmacol 24, 5–12. Suppl D. [PubMed: 12575463]

Patil O, Kaple M, 2023. Sensory processing differences in individuals with Autism Spectrum disorder: a narrative review of underlying mechanisms and sensory-based interventions. Cureus. 10.7759/cureus.48020.

Pesonen H, Strömmer J, Li X, Parkkari J, Tarkka IM, Astikainen P, 2023. Magnetoencephalography reveals impaired sensory gating and change detection in older adults in the somatosensory system. Neuropsychologia 190, 108702. 10.1016/j.neuropsychologia.2023.108702. [PubMed: 37838067]

Poon C-S, Young DL, 2006. Nonassociative learning as gated neural integrator and differentiator in stimulus-response pathways. Behav. Brain Funct 2, 29. 10.1186/1744-9081-2-29. [PubMed: 16893471]

Proskovec AL, Spooner RK, Wiesman AI, Wilson TW, 2020. Local cortical thickness predicts somatosensory gamma oscillations and sensory gating: a multimodal approach. Neuroimage 214, 116749. 10.1016/j.neuroimage.2020.116749. [PubMed: 32199953]

Roberts G, Holmes N, Alexander N, Boto E, Leggett J, Hill RM, Shah V, Rea M, Vaughan R, Maguire EA, Kessler K, Beebe S, Fromhold M, Barnes GR, Bowtell R, Brookes MJ, 2019. Towards OPM-MEG in a virtual reality environment. Neuroimage 199, 408–417. 10.1016/j.neuroimage.2019.06.010. [PubMed: 31173906]

Schulz SE, Luszawski M, Hannah KE, Stevenson RA, 2023. Sensory gating in neurodevelopmental disorders: a scoping review. Res. Child Adolesc. Psychopathol 51, 1005–1019. 10.1007/s10802-023-01058-9. [PubMed: 37014483]

Schulze M, Lux S, Philipsen A, 2020. Sensory processing in adult ADHD–a systematic review.

Spooner RK, Wiesman AI, O'Neill J, Schantell MD, Fox HS, Swindells S, Wilson TW, 2020. Prefrontal gating of sensory input differentiates cognitively impaired and unimpaired aging adults with HIV. Brain Commun. 2. 10.1093/braincomms/fcaa080 fcaa080. [PubMed: 32954330]

Spooner RK, Taylor BK, Ahmad IM, Dyball KN, Emanuel K, Fox HS, Stauch KL, Zimmerman MC, Wilson TW, 2021a. Neural oscillatory activity serving sensorimotor control is predicted by superoxide-sensitive mitochondrial redox environments. Proc. Natl. Acad. Sci 118, e2104569118. 10.1073/pnas.2104569118.

Spooner RK, Taylor BK, L'Heureux E, Schantell M, Arif Y, May PE, Morsey B, Wang T, Ideker T, Fox HS, Wilson TW, 2021b. Stress-induced aberrations in sensory processing predict worse cognitive outcomes in healthy aging adults. Aging 13, 19996–20015. 10.18632/aging.203433. [PubMed: 34410999]

Spooner RK, Wiesman AI, Mills MS, O'Neill J, Robertson KR, Fox HS, Swindells S, Wilson TW, 2018. Aberrant oscillatory dynamics during somatosensory processing in HIV-infected adults. NeuroImage: Clin. 20, 85–91. 10.1016/j.nicl.2018.07.009. [PubMed: 30094159]

Spooner RK, Wiesman AI, Proskovec AL, Heinrichs-Graham E, Wilson TW, 2019. Rhythmic spontaneous activity mediates the age-related decline in somatosensory function. Cereb. Cortex 29, 680–688. 10.1093/cercor/bhx349. [PubMed: 29342238]

Staines WR, Black SE, Graham SJ, McIlroy WE, 2002. Somatosensory gating and recovery from stroke involving the thalamus. Stroke 33, 2642–2651. 10.1161/01.str.0000032552.40405.40. [PubMed: 12411655]

Stevenson CM, Wang F, Brookes MJ, Zumer JM, Francis ST, Morris PG, 2012. Paired pulse depression in the somatosensory cortex: associations between MEG and BOLD fMRI. Neuroimage 59, 2722–2732. 10.1016/j.neuroimage.2011.10.037. [PubMed: 22036680]

Thoma RJ, Hanlon FM, Huang M, Miller GA, Moses SN, Weisend MP, Jones A, Paulson KM, Irwin J, Cañive JM, 2007. Impaired secondary somatosensory gating in patients with Schizophrenia. Psychiatry Res. 151, 189–199. 10.1016/j.psychres.2006.10.011. [PubMed: 17412427]

Tierney TM, Alexander N, Mellor S, Holmes N, Seymour R, O'Neill GC, Maguire EA, Barnes GR, 2021. Modelling optically pumped magnetometer interference in MEG as a spatially

homogeneous magnetic field. Neuroimage 244, 118484. 10.1016/j.neuroimage.2021.118484. [PubMed: 34418526]

Trevarrow MP, Kleinsmith J, Taylor BK, Wilson TW, Kurz MJ, 2021. The somatosensory cortical activity in individuals with cerebral palsy displays an aberrant developmental trajectory. J. Physiol 599, 1281–1289. 10.1113/JP280400. [PubMed: 33296078]

Trevarrow MP, Lew BJ, Hoffman RM, Taylor BK, Wilson TW, Kurz MJ, 2022. Altered somatosensory cortical activity is associated with cortical thickness in adults with cerebral palsy: multimodal evidence from MEG/sMRI. Cereb. Cortex 32, 1286–1294. 10.1093/cercor/bhab293. [PubMed: 34416763]

Uusitalo MA, Ilmoniemi RJ, 1997. Signal-space projection method for separating MEG or EEG into components. Med. Biol. Eng. Comput 35, 135–140. [PubMed: 9136207]

Wiesman AI, Groff BR, Wilson TW, 2019. Frontoparietal networks mediate the behavioral impact of alpha inhibition in visual cortex. Cereb. Cortex 29, 3505–3513. 10.1093/cercor/bhy220. [PubMed: 30215685]

Wiesman AI, Heinrichs-Graham E, Coolidge NM, Gehringer JE, Kurz MJ, Wilson TW, 2017. Oscillatory dynamics and functional connectivity during gating of primary somatosensory responses. J. Physiol 595, 1365–1375. 10.1113/JP273192. [PubMed: 27779747]

Wiesman AI, Koshy SM, Heinrichs-Graham E, Wilson TW, 2020. Beta and gamma oscillations index cognitive interference effects across a distributed motor network. Neuroimage 213, 116747. [PubMed: 32179103]

Wiesman AI, Mundorf VM, Casagrande CC, Wolfson SL, Johnson CM, May PE, Murman DL, Wilson TW, 2021. Somatosensory dysfunction is masked by variable cognitive deficits across patients on the Alzheimer's disease spectrum. EBioMedicine 73, 103638. 10.1016/j.ebiom.2021.103638. [PubMed: 34689085]

Wiesman AI, Wilson TW, 2019. Alpha frequency entrainment reduces the effect of visual distractors. J. Cogn. Neurosci 31, 1392–1403. 10.1162/jocn_a_01422. [PubMed: 31059352]

Wiesman AI, Wilson TW, 2020b. Posterior alpha and gamma oscillations index divergent and superadditive effects of cognitive interference. Cereb. Cortex 30, 1931–1945. 10.1093/cercor/bhz214. [PubMed: 31711121]

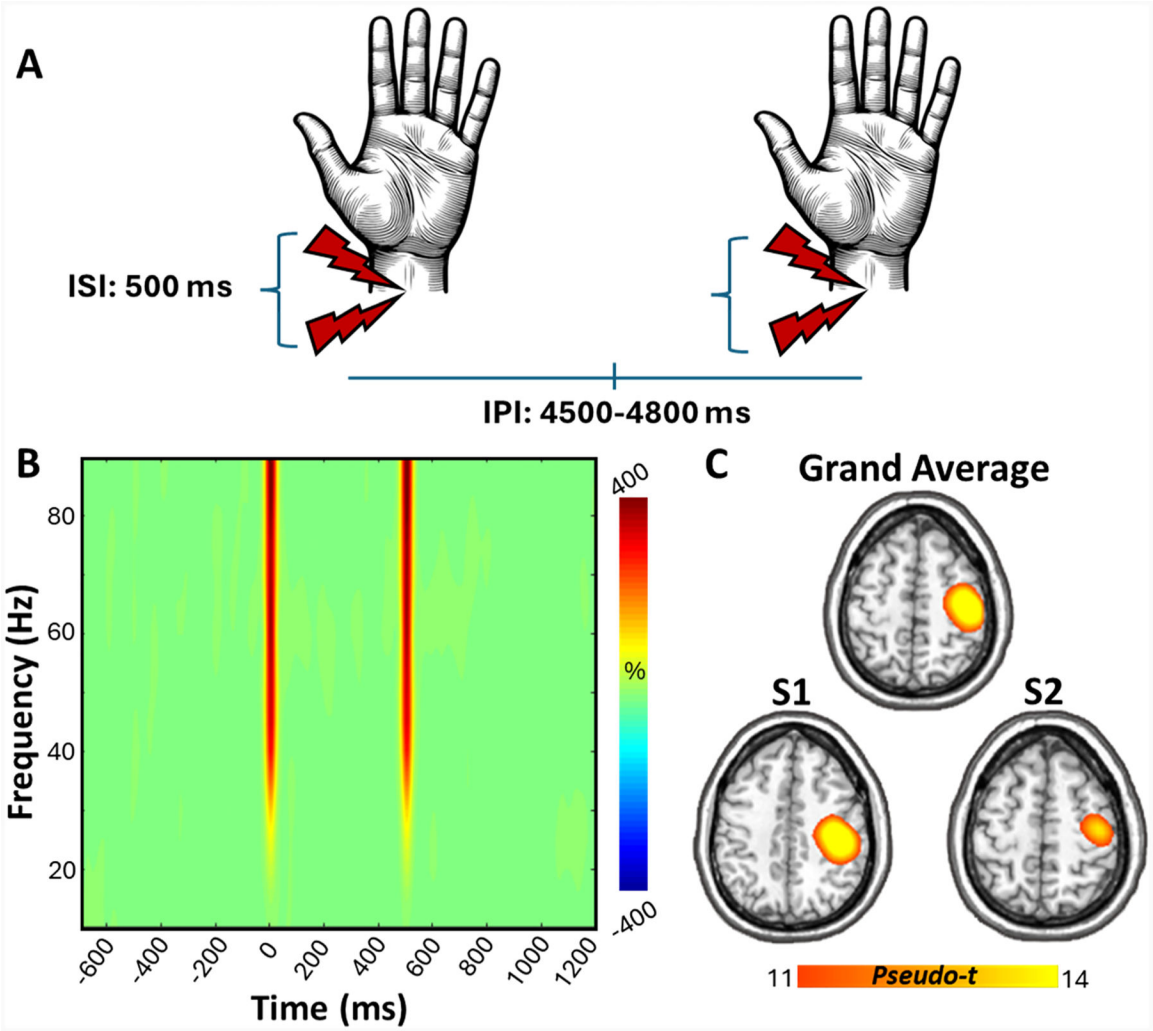

Fig. 1.

(A): **Median Nerve stimulation paradigm**: Each participant underwent somatosensory paired-pulse stimulation (inter-stimulus interval (ISI): 500 ms) of the median nerve of the nondominant left hand, separated by an inter-pair interval (IPI) of 4650 ± 150 ms. (B): **Time-frequency spectrogram:** Time-frequency responses to somatosensory stimulation from a sensor near the sensorimotor cortices, with time indicated in ms on the x-axis and frequency in Hz on the y-axis. Stimulations occurred at 0 and 500 ms. The percent change from baseline is indicated by the color bar to the right of the spectrogram. (C): **Neural responses in the primary somatosensory cortices**: Beamformer images (pseudo-t) for stimulation 1 (S1) and stimulation 2 (S2) with the group's grand average on the top. Strong increases in power were found in virtually identical areas of the contralateral hand region of the somatosensory cortices across all participants. ISI; inter-stimulus interval, IPI; inter-pair interval.

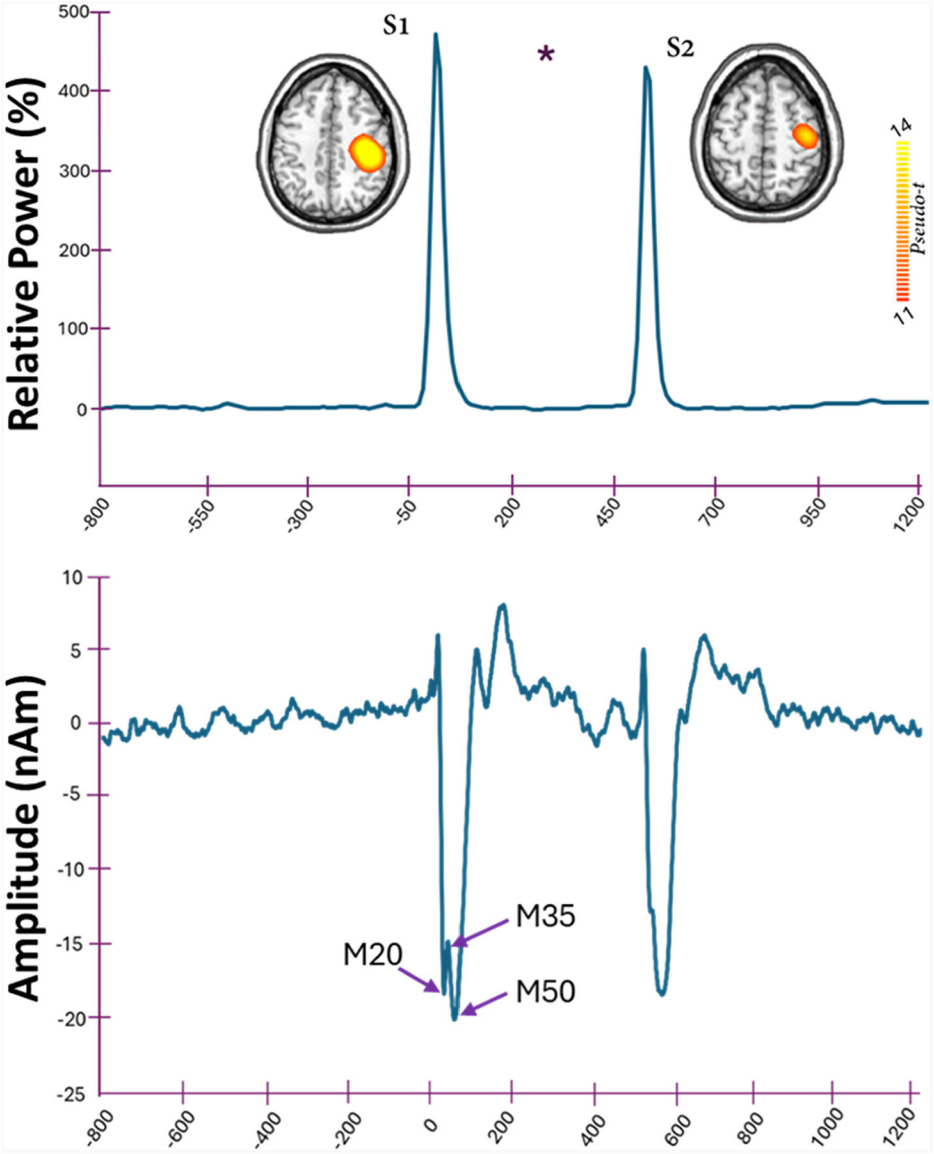

Fig. 2.

Baseline-normalized (i.e., relative) power envelope for the 30–75 Hz band. (Top): Time-frequency voxel time series revealed a significantly weaker response to the second stimulation (S2) compared to the first (S1), indicative of significant somato-SG in all participants. Relative power in percentage is shown on the y-axis with time in ms denoted on the x-axis. Averaged beamformer functional images per stimulation are shown with the respective neural responses. **Time-domain average of the somatosensory response (bottom):** Time-domain voxel time series showed M20, M35, and M50 components of the somatosensory responses with the amplitude (nAm) shown on the y-axis and time in ms on the x-axis. *$p < .05$.

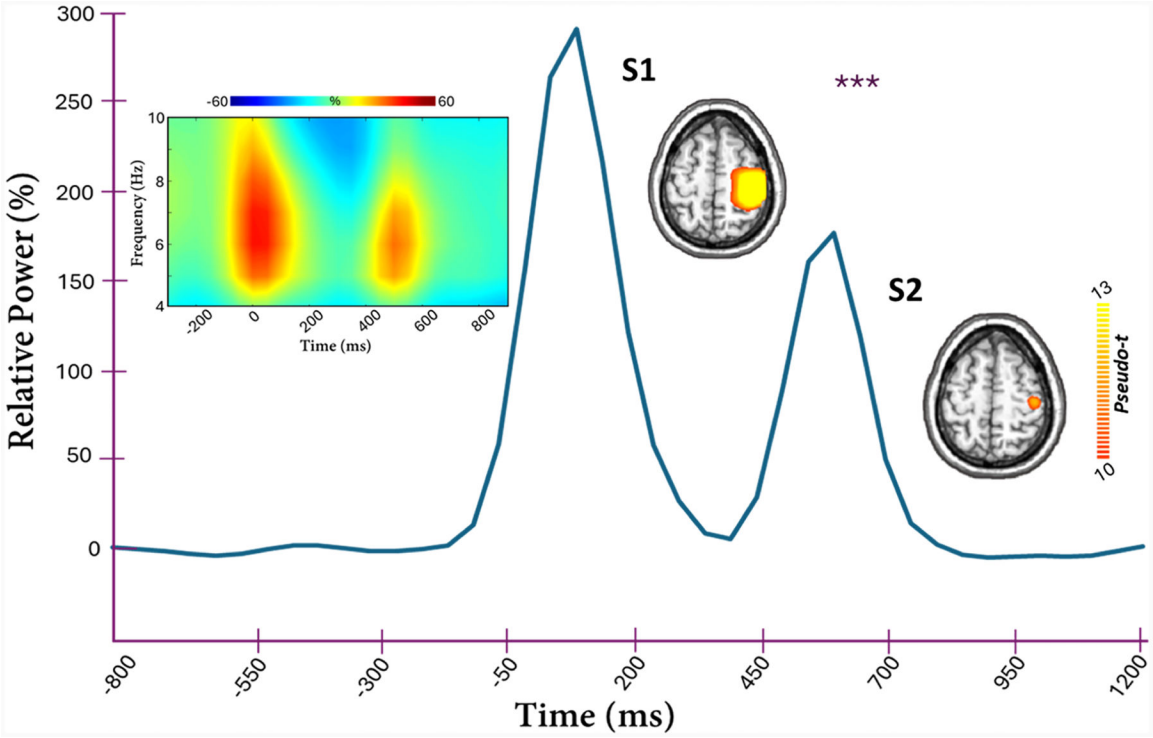

Fig. 3. Baseline-normalized (i.e., relative) power envelope for the theta band (4–8 Hz).

The top-left panel shows the time-frequency spectrogram. The time-frequency voxel time series revealed a significantly weaker response to the second stimulation (S2) compared to the first (S1), indicating robust somatosensory gating (somato-SG) across all participants. The y-axis represents relative power (in%), and the x-axis denotes time (in ms). Note that the early increase in the time series (i.e., before 0 ms) is due to plotting the envelope of a low frequency response (e.g., theta), which has a temporally smearing effect on the signal power. Averaged beamformer functional images are shown for each stimulation, illustrating the corresponding neural responses. *** $p < .001$.

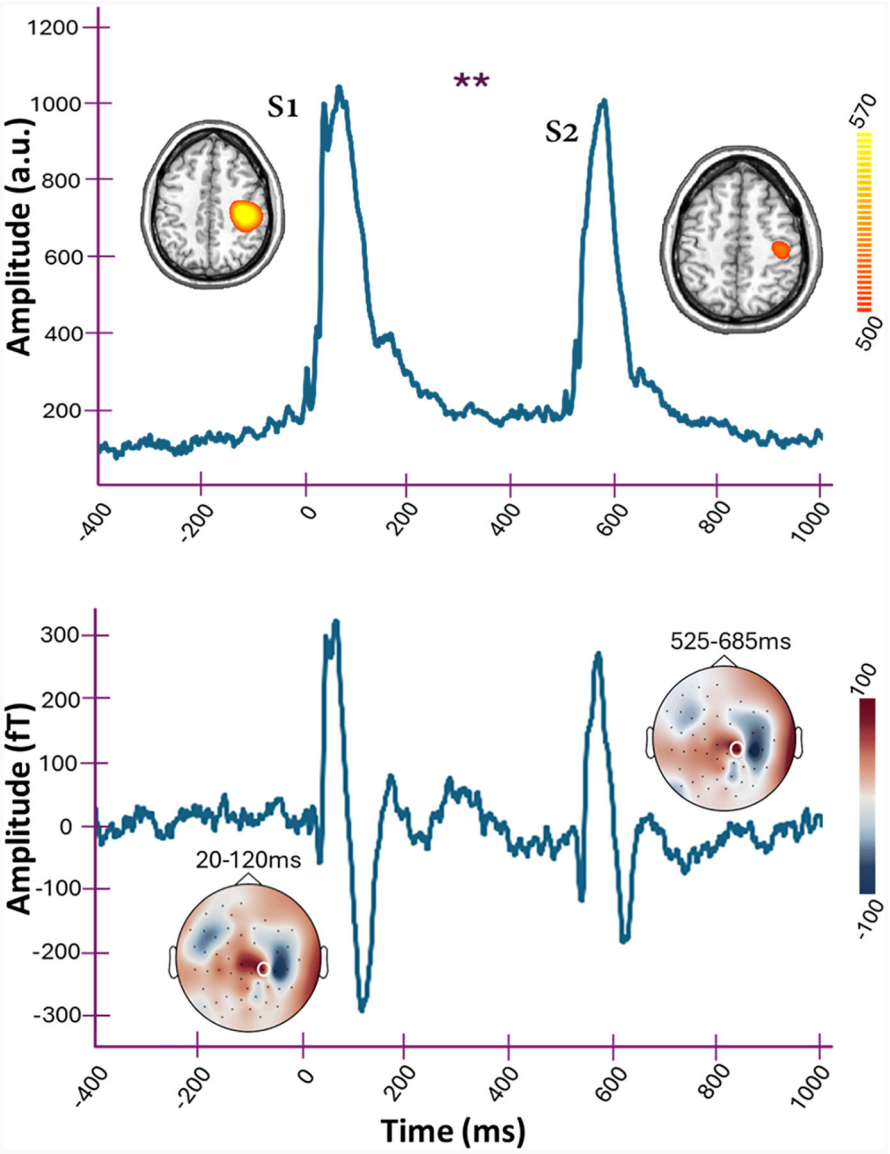

Fig. 4.

Time-domain somatosensory gating response (top): The time-domain averaged data across all participants extracted from the peak voxel of the grand-averaged sLORETA images showed robust responses to each stimulation, with the second stimulation (S2) being significantly weaker than the first (S1). The y-axis denotes amplitude in arbitrary units, while time in ms is represented on the x-axis. The sLORETA functional images per stimulation are shown with the neural responses. **Event-related field (bottom):** The time domain averaged activity from a representative magnetometer (i.e., JV; encircled in the topographic plots) is expressed in femto-Tesla (fT), with time in ms on the x-axis. The sensor-level topographic images are shown S1 (20–180 ms) and S2 (525–685 ms). ** $p <$ .005.